arXiv:2002.06130v1 [cond-mat.supr-con] 14 Feb 2020

Thermodynamic Evidence for a Two-Component Superconducting Order Parameter in Sr_2RuO_4

Sayak Ghosh,[1] Arkady Shekhter,[2] F. Jerzembeck,[3] N. Kikugawa,[4] Dmitry A. Sokolov,[3] Manuel Brando,[3] A. P. Mackenzie,[3] Clifford W. Hicks,[3] and B. J. Ramshaw*[1]

[1] *Laboratory of Atomic and Solid State Physics, Cornell University, Ithaca, NY 14853, USA*

[2] *National High Magnetic Field Laboratory, Florida State University, Tallahassee, FL 32310, USA*

[3] *Max Planck Institute for Chemical Physics of Solids, Dresden, Germany*

[4] *National Institute for Materials Science, Tsukuba, Ibaraki 305-0003, Japan*

ABSTRACT

Sr_2RuO_4 has stood as the leading candidate for a spin-triplet superconductor for 26 years. Recent NMR experiments have cast doubt on this candidacy, however, and it is difficult to find a theory of superconductivity that is consistent with all experiments. What is needed are symmetry-based experiments that can rule out broad classes of possible superconducting order parameters. Here we use resonant ultrasound spectroscopy to measure the entire symmetry-resolved elastic tensor of Sr_2RuO_4 through the superconducting transition. We observe a thermodynamic discontinuity in the shear elastic modulus c_{66}, requiring that the superconducting order parameter is two-component. A two-component p-wave order parameter, such as $p_x + ip_y$, naturally satisfies this requirement. As this order parameter appears to be precluded by recent NMR experiments, we suggest that two other two-component order parameters, namely $\{d_{xz}, d_{yz}\}$ or $\left\{d_{x^2-y^2}, g_{xy(x^2-y^2)}\right\}$, are now the prime candidates for the order parameter of Sr_2RuO_4.

INTRODUCTION

Nearly all known superconductors are "spin-singlet", composed of Cooper pairs that pair spin-up electrons with their spin-down counterparts. Noting that Sr_2RuO_4 has similar normal-state properties to superfluid ^{3}He, Rice and Sigrist[1] and, separately, Baskaran [2], suggested that Sr_2RuO_4 may be a solid-state "spin-triplet" superconductor. This attracted the attention of the experimental community, and ensured decades of intense research on Sr_2RuO_4, resulting in an extremely detailed understanding of its metallic state [3–6]. From this well-understood starting point one might expect the superconductivity of Sr_2RuO_4 to be a solved problem [7], but decades after its discovery the symmetry of the superconducting order parameter remains a mystery, largely due to discrepancies between several major pieces of experimental evidence[8].

Formerly, the strongest evidence for spin-triplet pairing in Sr_2RuO_4 was that the Knight shift was unchanged upon entering the superconducting state [9], suggesting that the Cooper pairs are composed of like-spin paired electrons. A recently revised version of this exper-

iment, however, has shown that the Knight shift is indeed suppressed below T_c, ruling against most spin-triplet order parameters [10, 11]. This is consistent with measurements of the upper-critical magnetic field, which appears to be Pauli-limited and thus suggests spin-singlet pairing [12]. The challenge is to reconcile these data with previous evidence in favour of a spin-triplet order parameter, including time-reversal symmetry breaking below T_c in μSR[13] and polar Kerr effect experiments[14], and half-quantized vortices [15].

While the spin-triplet versus spin-singlet aspect of the superconductivity in Sr_2RuO_4 is still under debate, less well studied is the symmetry of the orbital part of the Cooper pair wavefunction. By symmetry, spin-triplet superconductors are required to have an odd-parity orbital wavefunction, i.e. to be an $l = 1$ 'p-wave' or $l = 3$ 'f-wave' superconductor, where l is the orbital quantum number. This is in contrast with conventional $l = 0$ s-wave superconductors, or the high-T_c $l = 2$ d-wave superconductors. While some information about the orbital wavefunction can be inferred by looking for nodes in the superconducting gap, true momentum-space resolution of the nodes is difficult to achieve, and nodal position does not uniquely determine the orbital structure of the Cooper pair.

One way to distinguish different orbital states is by their degeneracy—the number of equivalent configurations with the same energy. s-wave and $d_{x^2-y^2}$-wave Cooper pairing states, for example, are both singly degenerate ("one-component"), while the more exotic $\{p_x, p_y\}$ state (which can order in the chiral $p_x + ip_y$ configuration) is two-fold degenerate ("two-component"). This difference in orbital degeneracy has a distinct signature in an ultrasound experiment—shear elastic moduli should be continuous through T_c for a singly-degenerate orbital state, but can have a discontinuity at T_c for a doubly degenerate state [16, 17]. The observation of a discontinuity in one of the shear elastic moduli of Sr_2RuO_4 at T_c would therefore constitute strong evidence in favour of either p-wave superconductivity, or one of the other more exotic two-fold degenerate superconducting order parameters. These measurements have been attempted in the past and were suggestive of a shear discontinuity at T_c, but a discontinuity was also found in a symmetry-forbidden channel, and the experimental resolution was deemed insufficient to be conclusive [18]. Other early evidence of a discontinuity in c_{66} [19] is now being submitted as part of a separate complementary study using an experimental technique different from our own.

EXPERIMENT

Ultrasound is a powerful tool for resolving questions of symmetry. First, elastic moduli are thermodynamic quantities, which means that they are truly indicative of ground-state properties, and can simply be calculated as second derivatives of the free energy with respect to strain. Secondly, because strain is a second-rank tensor, it can couple to order parameters in ways that lower-rank quantities, such as temperature and electric field, cannot. This endows ultrasound with a sensitivity to some of the symmetry properties of an order parameter, such as whether it has one or two components. Here we provide a brief overview of the connection between crystal symmetry, order parameter symmetry, and ultrasound: the detailed derivations can be found in the SI, as well as in a number of theoretical papers [16, 20–22].

Sr_2RuO_4 crystallizes in the tetragonal space group $I4/mmm$, along with its associated point group D_{4h}. In this crystal field environment, the five-component d-representation breaks into three one-component representations d_{z^2}, d_{xy}, and $d_{x^2-y^2}$ (the latter being the familiar 'd-wave' of the cuprates), and one two-component representation $\{d_{xz}, d_{yz}\}$. The three-component p-representation breaks into the one-component p_z representation and the two-component $\{p_x, p_y\}$ representation—it is this latter representation that has been proposed to order into the chiral $p_x + ip_y$ superconducting state in Sr_2RuO_4.

As illustrated in Figure 1, there are five unique strains (ϵ_Γ) in Sr_2RuO_4 (five irreducible representations of strain in D_{4h}): two compressive strains transforming as the A_{1g} representation, and three shear strains transforming as the B_{1g}, B_{2g} and E_g representations. Corresponding to each of these strains (labeled by its representation Γ), an elastic modulus $c_\Gamma = \partial^2\mathcal{F}/\partial\epsilon_\Gamma^2$ can be defined, where $\mathcal{F}$ is the thermodynamic free energy (sound velocities are then given as $v_\Gamma = \sqrt{c_\Gamma/\rho}$, where ρ is the density). When composing terms in the free energy, direct (linear) couplings between strain and superconducting order parameters (η) are never allowed because superconductivity breaks gauge symmetry. The next relevant coupling is linear in strain and quadratic in order parameter. For one-component superconducting order parameters, including all s-wave states and the $d_{x^2-y^2}$ state, the only quadratic form is η^2, and thus the only allowed coupling is $\epsilon_{A_{1g}}\eta^2$. This coupling produces discontinuities in all the A_{1g} (compressional) elastic moduli through T_c (see SI for details). Two-component order parameters ($\vec{\eta} = \{\eta_x, \eta_y\}$), however, have three quadratic forms: $\eta_x^2 + \eta_y^2$, $\eta_x^2 - \eta_y^2$,

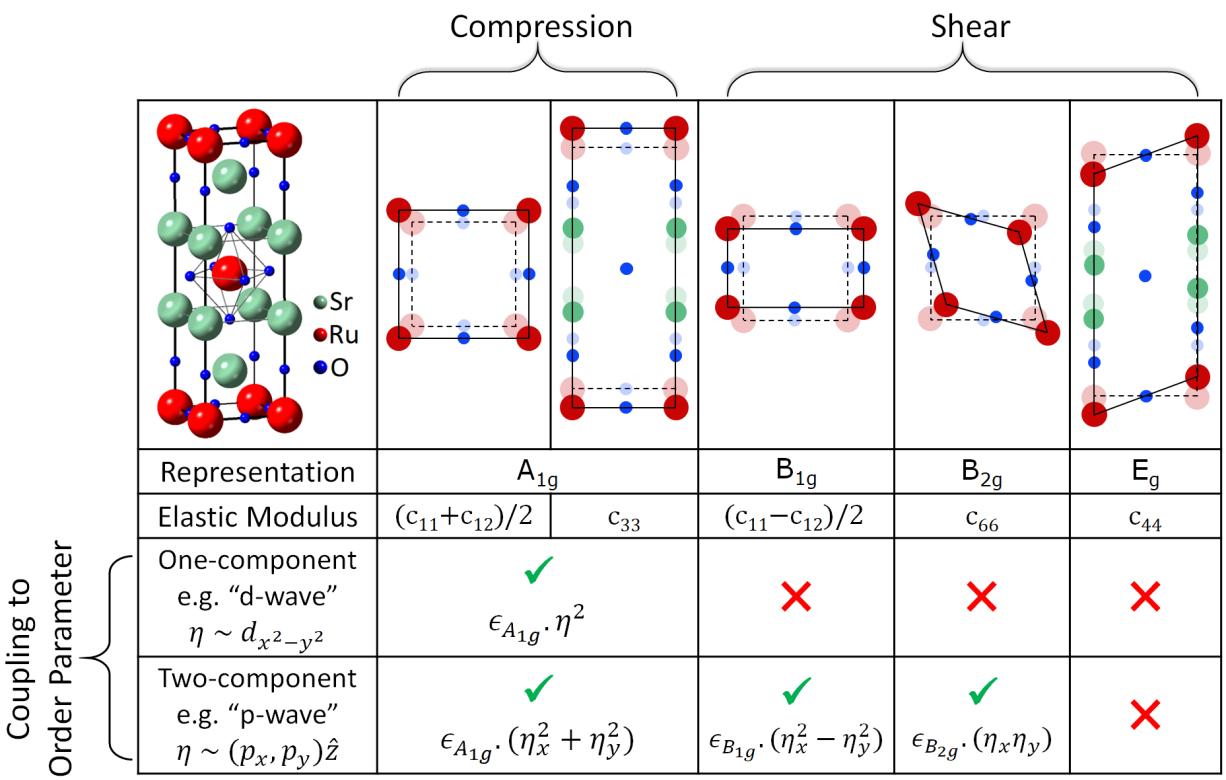

FIG. 1. **Irreducible strains in Sr_2RuO_4 and their coupling to superconducting order parameters.** The tetragonal crystal structure of Sr_2RuO_4 and unit cell deformations illustrating the irreducible representations of strain are shown. There is an elastic modulus corresponding to each of these strains, and a sixth modulus c_{13} that arises from coupling between the two A_{1g} strains. Green check marks denote allowed linear-order couplings to strain for one and two-component order parameter bilinears, and red crosses denote that such coupling is forbidden. These couplings are what lead to discontinuities in the elastic moduli at T_c. See Table I for a list of relevant possible order parameters in Sr_2RuO_4.

and $\eta_x\eta_y$, transforming as A_{1g}, B_{1g}, and B_{2g}, respectively. Thus in addition to coupling to the A_{1g} elastic moduli, two-component order parameters can couple to two of the shear moduli through $\epsilon_{B_{1g}}\left(\eta_x^2-\eta_y^2\right)$ and $\epsilon_{B_{2g}}\eta_x\eta_y$. This produces discontinuities in the associated shear elastic moduli ($(c_{11}-c_{12})/2$ and c_{66}, respectively), based purely on symmetry considerations, and independent of the microscopic mechanism of superconductivity.

While traditional ultrasound experiments measure a single elastic modulus per experiment, we use resonant ultrasound spectroscopy (RUS) to measure all six elastic moduli of Sr_2RuO_4 through T_c in a single experiment, greatly reducing systematic errors [23]. Analo-

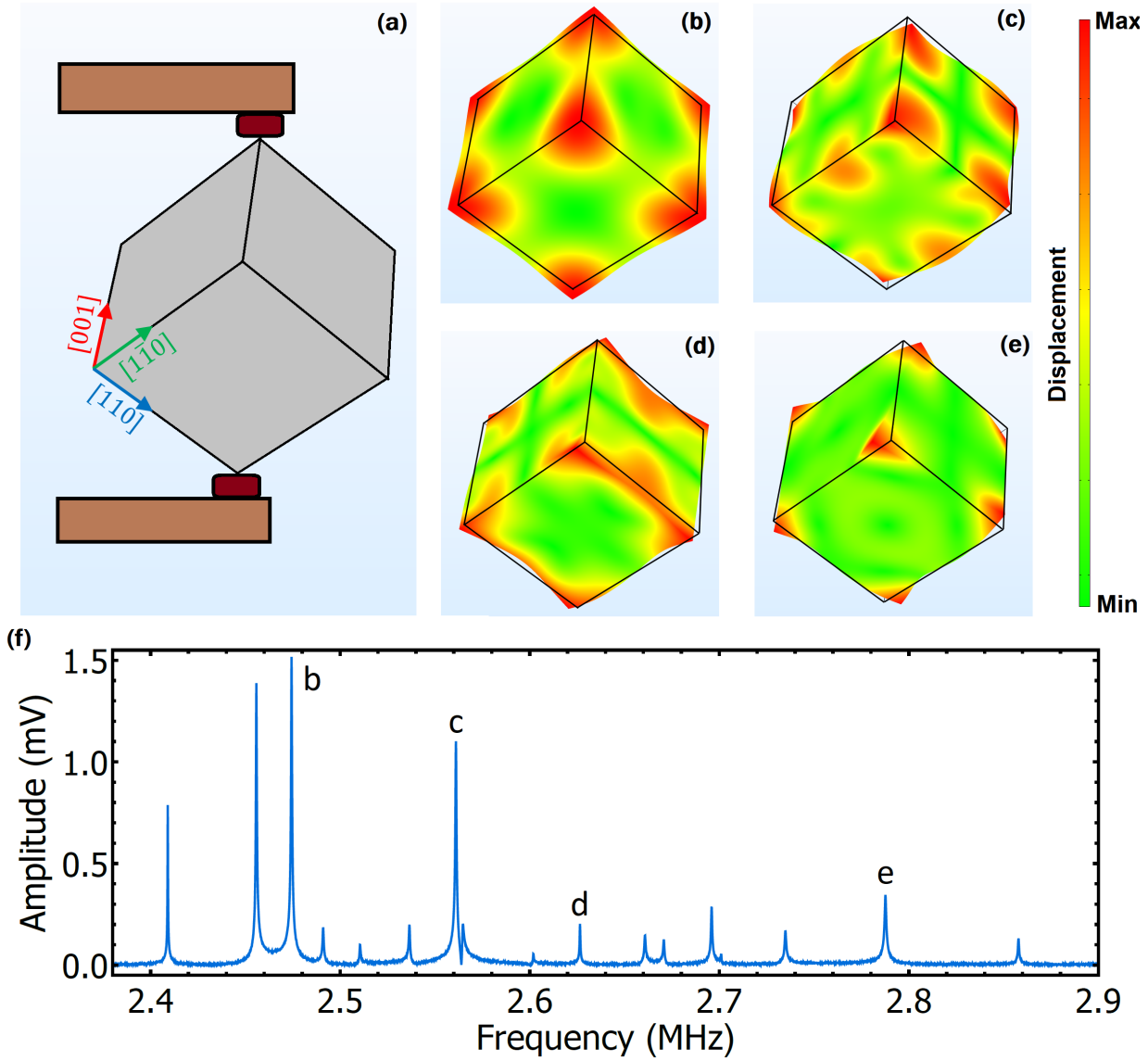

FIG. 2. **Resonant ultrasound spectroscopy: schematic and spectrum.** (a) A single-crystal sample, polished along known crystal axes, is held in weak-coupling contact between two ultrasonic transducers, allowing it to vibrate freely at its resonance frequencies. Panels (b) through (e) show the crystal's deformation corresponding to four particular experimentally measured resonances, marked in (f). (f) A portion of the ultrasonic spectrum of Sr_2RuO_4 in the frequency range 2.4-2.9 MHz, taken at room temperature. Each resonance creates a unique strain pattern in the material that can be decomposed in terms of the five irreducible strains (Figure 1(a)), modulated in phase along the dimensions of the sample.

gous to how a stretched string has standing waves that can be expressed in terms of sinusoidal harmonics, three-dimensional solids have elastic resonances that can be decomposed in terms of irreducible representations of strain (shown in Figure 2). RUS measures the frequencies of these resonances for a single crystal sample, from which all elastic moduli can be obtained by inverse-solving the elastic wave equation [24]. The relatively low T_c (≈ 1.43 K for our sample) of Sr_2RuO_4, however, poses technical challenges to perform RUS experiments through the superconducting transition. RUS samples are typically large (~ 1 mm^3), and ideally are only held by their corners—in weak-coupling contact with the transducers (see Figure 2(a)). This ensures nearly-free boundary conditions—required for the data analysis—but prevents good thermal coupling between the apparatus and the sample. Previous RUS implementations either sacrificed uniform cooling by placing the sample in vacuum [24], or sacrificed a slow cooling rate by placing the sample in direct thermal contact with the helium bath [25]. Our new RUS design employs a double-vacuum can arrangement to allow for slow, uniform cooling of a sample down to ~ 1.25 K. We observe a sharp (40 mK wide) superconducting transition (Figure 3(a)), signifying high sample quality and uniform cooling.

We performed RUS measurements of the free elastic resonances of a single-crystal sample of Sr_2RuO_4 through T_c, five examples of which are shown in Figure 3(a). We decomposed 18 such resonances into the five irreducible elastic moduli (plus the sixth modulus c_{13}, which couples the two A_{1g} strains together), the temperature evolution of which is shown in Figure 3(b) and (c). Discontinuities are clearly observed in all three compressional (A_{1g}) moduli, as required by thermodynamics for all superconductors, as well as in the shear modulus c_{66} (B_{2g}). The discontinuity in c_{66} is forbidden by symmetry for one-component order parameters, but is allowed for two-component order parameters—this discontinuity is our central finding.

Because RUS provides access to all elastic moduli through T_c, there are a few consistency checks we can perform on our data. Firstly, the coupling between strains and the order parameter is constrained by symmetry such that c_{44} may not have a discontinuity at T_c for any superconducting order parameter. We observe only a change in $\partial c_{44}/\partial T$ at T_c: this is due to the blinear coupling $\epsilon^2\eta^2$ that is allowed for all strain-order parameter pairs. Secondly, discontinuities in the three A_{1g} moduli should follow a self-consistency relation derived from

a general Landau-Ginzburg analysis for a second order phase transition (see S.I.),

$$(\Delta\frac{c_{11}+c_{12}}{2})\times(\Delta c_{33})=(\Delta c_{13})^2. \tag{1}$$

We obtain $(\Delta\frac{c_{11}+c_{12}}{2})\times(\Delta c_{33})=(8\pm1)\times10^{-5}$ GPa^2 and $(\Delta c_{13})^2=(7\pm1)\times10^{-5}$ GPa^2. Both of these consistency checks validate our approach of analyzing the discontinuities at T_c using a Ginzburg-Landau type expansion in powers of the order parameter and strain.

A further check on the data is provided by the Ehrenfest relations that relate the derivative of T_c with hydrostatic pressure P to the discontinuities at T_c in the specific heat, ΔC, and the bulk modulus, ΔB, via

$$\left(\frac{dT_c}{dP}\right)^2=-\frac{\Delta B}{B^2}\left(\frac{\Delta C}{T}\right)^{-1}. \tag{2}$$

Using our measurement of the full elastic tensor we compute a discontinuity in the bulk modulus of $\Delta B/B\approx5.9\times10^{-5}$ (see S.I.). Combining this with the measured value of specific heat for this sample (see S.I.), Equation 2 yields a value for dT_c/dP of 0.87 K/GPa—a factor of 2.9 higher than what has been reported [26]. This apparent discrepancy may be resolved by the fact that there appear to be two transitions occurring at or near the superconducting T_c, as discovered in recent μSR experiments [27]. The two transition temperatures split apart when stress is applied along the x direction—Meissner screening onsets at the higher of the two transitions, T_c, while time reversal symmetry appears to be broken at the lower transition, T_{TRSB} . To perform the correct Ehrenfest analysis one would require dT_{TRSB}/dP, in addition to the known value of dT_c/dP.

DISCUSSION

A discontinuity in c_{66} at T_c requires that the superconducting order parameter be of two-component type (see Table I). This is a critical piece of information because evidence for vertical line nodes in the superconducting gap—from ultrasonic attenuation [28], heat capacity [29], thermal conductivity [30], and quasiparticle interference [31]—are most straightforwardly interpreted in terms of a one-component, $d_{x^2-y^2}$ order parameter. With the recently-discovered suppression of the Knight shift strongly suggesting that the order parameter cannot be spin-triplet [10], $d_{x^2-y^2}$ would seem a likely contender. The discontinuity in c_{66}, however, rules against any one-component order parameter, including $d_{x^2-y^2}$.

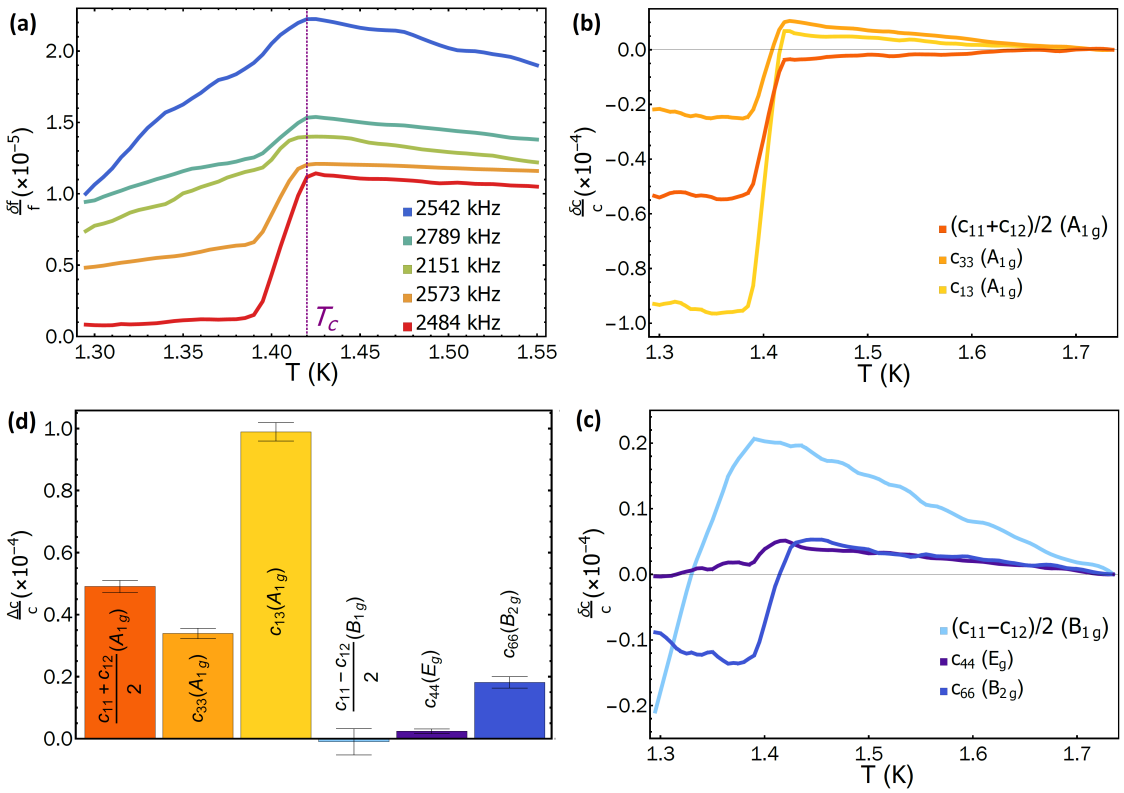

FIG. 3. **Resonant ultrasound spectroscopy through T_c in Sr_2RuO_4.** (a) Temperature evolution of five representative resonances measured through T_c— plots are shifted vertically for visual clarity. Dashed line shows T_c determined from resistivity measurements. A step-like discontinuity ("jump") is observed at T_c—the different magnitudes of this discontinuity signify the contributions of different elastic moduli in each resonance. 18 such resonances were tracked through T_c to determine the elastic moduli. (b) Compressional (A_{1g}) and (c) shear (B_{1g}, E_g and B_{2g}) moduli of Sr_2RuO_4 through T_c. The absolute values of these moduli at 4 kelvin are determined to be $(c_{11}+c_{12})/2 = 190.8$, $c_{33} = 257.2$, $c_{13} = 85.0$, $(c_{11}-c_{12})/2 = 53.1$, $c_{66} = 65.5$ and $c_{44} = 69.5$ GPa. (d) Magnitudes of the elastic moduli jumps at T_c, along with their experimental uncertainties.

We propose that our result, combined with the presence of nodal quasiparticles, time reversal symmetry breaking, and suppression of the Knight shift, leaves two likely remaining possibilities: $d_{xz} \pm id_{yz}$, and $d_{x^2-y^2} \pm ig_{xy(x^2-y^2)}$. Other two component order parameters, such as $d_{x^2-y^2} + is$ [32], do not produce a discontinuity in c_{66}. The absence of a discontinuity in $(c_{11} - c_{12})/2$, on the face of it, implies that there is no order parameter bilinear that transforms as B_{2g}, ruling out $d_{xz} \pm id_{yz}$. It is possible, however, that while a jump in $(c_{11} - c_{12})/2$ is allowed thermodynamically, it is either unobservably small because the cou-

Dimensionality	Order Parameter	Representation	Moduli Jumps
One-component	s	A_{1g}	A_{1g}
	$d_{x^2-y^2}$	B_{1g}	A_{1g}
	d_{xy}	B_{2g}	A_{1g}
Two-component	$\{p_x, p_y\}\,\hat{\boldsymbol{z}}$	E_u	A_{1g}, B_{1g}, B_{2g}
	$p_z\,\{\hat{\boldsymbol{x}}, \hat{\boldsymbol{y}}\}$	E_u	A_{1g}, B_{1g}, B_{2g}
	$\{d_{xz}, d_{yz}\}$	E_g	A_{1g}, B_{1g}, B_{2g}
	$\{d_{x^2-y^2}, g_{xy(x^2-y^2)}\}$	$B_{1g} \oplus A_{2g}$	A_{1g}, B_{2g}

TABLE I. **Some superconducting order parameters and their representations in D_{4h}.** For the odd-parity spin-triplet order parameters, $\hat{\boldsymbol{x}}$, $\hat{\boldsymbol{y}}$ and $\hat{\boldsymbol{z}}$ represent the pair wavefunction in spin space in the **d**-vector notation [7]. Two component order parameters $\{\eta_x, \eta_y\}$ can order as η_x, η_y, $\eta_x \pm \eta_y$, or $\eta_x \pm i\eta_y$, depending on microscopic details. It is this latter combination that forms the time-reversal symmetry breaking state (e.g. $(p_x + ip_y)\hat{\boldsymbol{z}}$, or $d_{xz} + id_{yz}$). Only two-component OPs are consistent with the jump we find at T_c in c_{66}. Note that the $B_{1g} \oplus A_{2g}$ order does not belong to a single representation of D_{4h}, and thus transition temperatures of the d and g components must be "fine-tuned" if they are to coincide.

pling coefficient is small (for microscopic reasons), or is smeared-out due to the to the high ultrasonic attenuation in the B_{1g} elastic channel [33]. Thus we will consider the implications of both a $d_{xz} \pm id_{yz}$ and a $d_{x^2-y^2} \pm ig_{xy(x^2-y^2)}$ superconducting state in Sr_2RuO_4.

The first of these, $d_{xz} \pm id_{yz}$, is the chiral-ordered state of $\{d_{xz}, d_{yz}\}$—a two-component E_g representation [34]. There are two main arguments against such a state. First, $\{d_{xz}, d_{yz}\}$ has a horizontal line node at $k_z = 0$, whereas the nodes in Sr_2RuO_4 are thought to lie along the [110] and [$\bar{1}$10] directions [28–31]. Second, Sr_2RuO_4 has very weak interlayer coupling [6], and in the limit of weak interlayer coupling the pairing strength for this state goes to zero. A recent weak-coupling analysis, however, shows that an E_g state can be stabilized by including momentum-dependent spin orbit coupling [35, 36], and such spin-orbit coupling has been quantified by ARPES in Sr_2RuO_4 [37, 38]. This variant of the E_g state has Bogoliubov Fermi surfaces rather than line nodes, extending along the k_z direction in a manner such that they may mimic line-nodes as far as experiment is concerned.

The second possibility, $d_{x^2-y^2} \pm ig_{xy(x^2-y^2)}$, is less natural in that $d_{x^2-y^2}$ is a B_{1g} repre-

sentation and $g_{xy(x^2-y^2)}$ is an A_{2g} representation [39]. Order parameters of different representations are allowed (within a Ginzburg-Landau treatment) to have distinct transition temperatures, and thus this composite $\mathrm{B}_{1g} \oplus \mathrm{A}_{2g}$ order parameter requires fine-tuning to produce a single superconducting transition. Fine-tuning aside, this state has two attractive features. First, it produces bilinears only in the A_{1g} and B_{2g} channels ($\mathrm{B}_{1g} \otimes A_{2g} = \mathrm{B}_{2g}$). This could naturally explain why a jump is seen in c_{66} but not in $(c_{11} - c_{12})/2$. Second, this state has line nodes exactly along the [110] and [$\bar{1}$10] directions [28, 30, 31]. While the $l = 4$, $g_{xy(x^2-y^2)}$ state may seem exotic, it has been shown to be competitive with $d_{x^2-y^2}$ within weak coupling when nearest-neighbor repulsion is accounted for [40].

Both of these two-component order parameters produce a discontinuity in c_{66}, break time reversal symmetry, are Pauli limited in their upper critical field, exhibit a drop in the Knight shift below T_c, and have ungapped quasiparticles. The accidental degeneracy of $d_{x^2-y^2} \pm ig_{xy(x^2-y^2)}$ means that T_c should split into two transitions under *any* applied strain, and indeed, the aforementioned μSR measurements have found evidence for such a splitting [27]. This suggests that $\mathrm{Sr_2RuO_4}$ may indeed have two nearly degenerate transitions at ambient pressure. Whether or not such a fine-tuned state is tenable to all experiments remains to be seen, but it is becoming clear that a two-component superconducting order parameter is the right framework in which to understand the unusual superconducting properties of $\mathrm{Sr_2RuO_4}$.

ACKNOWLEDGMENTS

B.J.R. and S.G. are grateful for help with the experimental design from Eric Smith, Jeevak Parpia, and the LASSP machine shop. B.J.R and S.G. acknowledge support from the U.S. Department of Energy, Office of Basic Energy Sciences under Award Number DE-SC0020143. N.K. acknowledges the support from JSPS KAKENHI (No. JP18K04715) in Japan.

[1] T. M. Rice and M. Sigrist. $\mathrm{Sr_2RuO_4}$: an electronic analogue of ^{3}He? *Journal of Physics: Condensed Matter*, 7(47):L643–L648, nov 1995. doi:10.1088/0953-8984/7/47/002.

[2] G Baskaran. Why is sr2ruo4 not a high tc superconductor? electron correlation, hund's coupling and p-wave instability. *Physica B: Condensed Matter*, 223:490–495, 1996.

[3] Yoshiteru Maeno, Koji Yoshida, Hiroaki Hashimoto, Shuji Nishizaki, Shin-ichi Ikeda, Minoru Nohara, Toshizo Fujita, Andrew P. Mackenzie, Nigel E. Hussey, J. Georg Bednorz, and Frank Lichtenberg. Two-dimensional fermi liquid behavior of the superconductor Sr_2RuO_4. *Journal of the Physical Society of Japan*, 66(5):1405–1408, 1997. doi:10.1143/JPSJ.66.1405. URL `https://doi.org/10.1143/JPSJ.66.1405`.

[4] N. E. Hussey, A. P. Mackenzie, J. R. Cooper, Y. Maeno, S. Nishizaki, and T. Fujita. Normal-state magnetoresistance of Sr_2RuO_4. *Phys. Rev. B*, 57:5505–5511, Mar 1998. doi:10.1103/PhysRevB.57.5505. URL `https://link.aps.org/doi/10.1103/PhysRevB.57.5505`.

[5] D. Stricker, J. Mravlje, C. Berthod, R. Fittipaldi, A. Vecchione, A. Georges, and D. van der Marel. Optical response of Sr_2RuO_4 reveals universal fermi-liquid scaling and quasiparticles beyond Landau theory. *Phys. Rev. Lett.*, 113:087404, Aug 2014. doi:10.1103/PhysRevLett.113.087404. URL `https://link.aps.org/doi/10.1103/PhysRevLett.113.087404`.

[6] C. Bergemann, S. R. Julian, A. P. Mackenzie, S. NishiZaki, and Y. Maeno. Detailed topography of the fermi surface of sr_2ruo_4. *Phys. Rev. Lett.*, 84:2662–2665, Mar 2000. doi:10.1103/PhysRevLett.84.2662. URL `https://link.aps.org/doi/10.1103/PhysRevLett.84.2662`.

[7] Andrew Peter Mackenzie and Yoshiteru Maeno. The superconductivity of Sr_2RuO_4 and the physics of spin-triplet pairing. *Rev. Mod. Phys.*, 75:657–712, May 2003. doi:10.1103/RevModPhys.75.657. URL `https://link.aps.org/doi/10.1103/RevModPhys.75.657`.

[8] Andrew P. Mackenzie, Thomas Scaffidi, Clifford W. Hicks, and Yoshiteru Maeno. Even odder after twenty-three years: the superconducting order parameter puzzle of Sr_2RuO_4. *npj Quantum Materials*, 2(1):40, 2017. ISSN 2397-4648. doi:10.1038/s41535-017-0045-4. URL `https://doi.org/10.1038/s41535-017-0045-4`.

[9] K. Ishida, H. Mukuda, Y. Kitaoka, K. Asayama, Z. Q. Mao, Y. Mori, and Y. Maeno. Spin-triplet superconductivity in sr2ruo4 identified by 17o knight shift. *Nature*, 396(6712):658–660, 1998. ISSN 1476-4687. doi:10.1038/25315. URL `https://doi.org/10.1038/25315`.

[10] A. Pustogow, Yongkang Luo, A. Chronister, Y.-S. Su, D. A. Sokolov, F. Jerzembeck, A. P. Mackenzie, C. W. Hicks, N. Kikugawa, S. Raghu, E. D. Bauer, and S. E. Brown. Constraints on the superconducting order parameter in sr2ruo4 from oxygen-17 nuclear magnetic resonance. *Nature*, 574(7776):72–75, 2019. ISSN 1476-4687. doi:10.1038/s41586-019-1596-2. URL `https://doi.org/10.1038/s41586-019-1596-2`.

[11] Kenji Ishida, Masahiro Manago, and Yoshiteru Maeno. Reduction of the ^{1}7o knight shift in the superconducting state and the heat-up effect by nmr pulses on sr_2ruo_4. *arXiv preprint arXiv:1907.12236*, 2019.

[12] S. Kittaka, T. Nakamura, Y. Aono, S. Yonezawa, K. Ishida, and Y. Maeno. Angular dependence of the upper critical field of sr_2ruo_4. *Phys. Rev. B*, 80:174514, Nov 2009. doi:10.1103/PhysRevB.80.174514. URL `https://link.aps.org/doi/10.1103/PhysRevB.80.174514`.

[13] G. M. Luke, Y. Fudamoto, K. M. Kojima, M. I. Larkin, J. Merrin, B. Nachumi, Y. J. Uemura, Y. Maeno, Z. Q. Mao, Y. Mori, H. Nakamura, and M. Sigrist. Time-reversal symmetry-breaking superconductivity in sr2ruo4. *Nature*, 394(6693):558–561, 1998. ISSN 1476-4687. doi:10.1038/29038. URL `https://doi.org/10.1038/29038`.

[14] Jing Xia, Yoshiteru Maeno, Peter T. Beyersdorf, M. M. Fejer, and Aharon Kapitulnik. High resolution polar kerr effect measurements of sr_2ruo_4: Evidence for broken time-reversal symmetry in the superconducting state. *Phys. Rev. Lett.*, 97:167002, Oct 2006. doi:10.1103/PhysRevLett.97.167002. URL `https://link.aps.org/doi/10.1103/PhysRevLett.97.167002`.

[15] J. Jang, D. G. Ferguson, V. Vakaryuk, R. Budakian, S. B. Chung, P. M. Goldbart, and Y. Maeno. Observation of half-height magnetization steps in sr2ruo4. *Science*, 331(6014):186–188, 2011. ISSN 0036-8075. doi:10.1126/science.1193839. URL `https://science.sciencemag.org/content/331/6014/186`.

[16] Walther Rehwald. The study of structural phase transitions by means of ultrasonic experiments. *Advances in Physics*, 22(6):721–755, 1973. doi:10.1080/00018737300101379.

[17] Sayak Ghosh, Michael Matty, Ryan Baumbach, Eric D. Bauer, K. A. Modic, Arkady Shekhter, J. A. Mydosh, Eun-Ah Kim, and B. J. Ramshaw. Single-Component Order Parameter in URu_2Si_2 Uncovered by Resonant Ultrasound Spectroscopy and Machine Learning. *arXiv e-prints*, art. arXiv:1903.00552, Mar 2019.

[18] Noriki Okuda, Takashi Suzuki, Zhiqiang Mao, Yoshiteru Maeno, and Toshizo Fujita. Unconventional strain dependence of superconductivity in spin-triplet superconductor sr2ruo4. *Journal of the Physical Society of Japan*, 71(4):1134–1139, 2002.

[19] C. Lupien. *Ultrasound attenuation in the unconventional superconductor Sr_2RuO_4*. PhD thesis, 2002.

[20] Manfred Sigrist and Kazuo Ueda. Phenomenological theory of unconventional superconductivity. *Rev. Mod. Phys.*, 63:239–311, Apr 1991. doi:10.1103/RevModPhys.63.239. URL `https://link.aps.org/doi/10.1103/RevModPhys.63.239`.

[21] Manfred Sigrist. Ehrenfest Relations for Ultrasound Absorption in Sr_2RuO_4. *Progress of Theoretical Physics*, 107(5):917–925, 05 2002. ISSN 0033-068X. doi:10.1143/PTP.107.917. URL `https://doi.org/10.1143/PTP.107.917`.

[22] Wen Huang, Yi Zhou, and Hong Yao. Possible 3D nematic odd-parity pairing in Sr_2RuO_4: experimental evidences and predictions. *arXiv e-prints*, art. arXiv:1901.07041, Jan 2019.

[23] A_ Migliori, JL Sarrao, William M Visscher, TM Bell, Ming Lei, Z Fisk, and R Gi Leisure. Resonant ultrasound spectroscopic techniques for measurement of the elastic moduli of solids. *Physica B: Condensed Matter*, 183(1-2):1–24, 1993.

[24] B. J. Ramshaw, Arkady Shekhter, Ross D. McDonald, Jon B. Betts, J. N. Mitchell, P. H. Tobash, C. H. Mielke, E. D. Bauer, and Albert Migliori. Avoided valence transition in a plutonium superconductor. *Proceedings of the National Academy of Sciences*, 112(11):3285–3289, 2015. ISSN 0027-8424. doi:10.1073/pnas.1421174112.

[25] R. G. Goodrich, David P. Young, Donavan Hall, Luis Balicas, Z. Fisk, N. Harrison, J. Betts, Albert Migliori, F. M. Woodward, and J. W. Lynn. Extension of the temperature-magnetic field phase diagram of ceb_6. *Phys. Rev. B*, 69:054415, Feb 2004. doi:10.1103/PhysRevB.69.054415. URL `https://link.aps.org/doi/10.1103/PhysRevB.69.054415`.

[26] D. Forsythe, S. R. Julian, C. Bergemann, E. Pugh, M. J. Steiner, P. L. Alireza, G. J. McMullan, F. Nakamura, R. K. W. Haselwimmer, I. R. Walker, S. S. Saxena, G. G. Lonzarich, A. P. Mackenzie, Z. Q. Mao, and Y. Maeno. Evolution of fermi-liquid interactions in sr_2ruo_4 under pressure. *Phys. Rev. Lett.*, 89:166402, Sep 2002. doi:10.1103/PhysRevLett.89.166402. URL `https://link.aps.org/doi/10.1103/PhysRevLett.89.166402`.

[27] Vadim Grinenko, Shreenanda Ghosh, Rajib Sarkar, Jean-Christophe Orain, Artem Nikitin, Matthias Elender, Debarchan Das, Zurab Guguchia, Felix Brckner, Mark E. Barber, Joonbum

Park, Naoki Kikugawa, Dmitry A. Sokolov, Jake S. Bobowski, Takuto Miyoshi, Yoshiteru Maeno, Andrew P. Mackenzie, Hubertus Luetkens, Clifford W. Hicks, and Hans-Henning Klauss. Split superconducting and time-reversal symmetry-breaking transitions, and magnetic order in sr_2ruo_4 under uniaxial stress. 2020.

[28] Christian Lupien. *Ultrasound attenuation in the unconventional superconductor Sr2RuO4*. PhD Thesis, 2002.

[29] Kazuhiko Deguchi, Z Q. Mao, and Yoshiteru Maeno. Determination of the superconducting gap structure in all bands of the spin-triplet superconductor sr _2 ruo _4. *Journal of the Physical Society of Japan*, 73(5):1313–1321, 2004.

[30] E. Hassinger, P. Bourgeois-Hope, H. Taniguchi, S. René de Cotret, G. Grissonnanche, M. S. Anwar, Y. Maeno, N. Doiron-Leyraud, and Louis Taillefer. Vertical line nodes in the superconducting gap structure of Sr_2RuO_4. *Phys. Rev. X*, 7:011032, Mar 2017. doi:10.1103/PhysRevX.7.011032. URL `https://link.aps.org/doi/10.1103/PhysRevX.7.011032`.

[31] Rahul Sharma, Stephen D. Edkins, Zhenyu Wang, Andrey Kostin, Chanchal Sow, Yoshiteru Maeno, Andrew P. Mackenzie, J. C. Samus Davis, and Vidya Madhavan. Momentum resolved superconducting energy gaps of sr_2ruo_4 from quasiparticle interference imaging, 2019.

[32] A. T. Rømer, D. D. Scherer, I. M. Eremin, P. J. Hirschfeld, and B. M. Andersen. Knight shift and leading superconducting instability from spin fluctuations in sr_2ruo_4. *Phys. Rev. Lett.*, 123:247001, Dec 2019. doi:10.1103/PhysRevLett.123.247001. URL `https://link.aps.org/doi/10.1103/PhysRevLett.123.247001`.

[33] C. Lupien, W. A. MacFarlane, Cyril Proust, Louis Taillefer, Z. Q. Mao, and Y. Maeno. Ultrasound attenuation in Sr_2RuO_4: An angle-resolved study of the superconducting gap function. *Phys. Rev. Lett.*, 86:5986–5989, Jun 2001. doi:10.1103/PhysRevLett.86.5986. URL `https://link.aps.org/doi/10.1103/PhysRevLett.86.5986`.

[34] Igor Žutić and Igor Mazin. Phase-sensitive tests of the pairing state symmetry in sr_2ruo_4. *Phys. Rev. Lett.*, 95:217004, Nov 2005. doi:10.1103/PhysRevLett.95.217004. URL `https://link.aps.org/doi/10.1103/PhysRevLett.95.217004`.

[35] Aline Ramires and Manfred Sigrist. The superconducting order parameter of Sr_2RuO_4: a microscopic perspective. *arXiv e-prints*, art. arXiv:1905.01288, May 2019.

[36] Han Gyeol Suh, Henri Menke, PMR Brydon, Carsten Timm, Aline Ramires, and Daniel F Agterberg. Stabilizing even-parity chiral superconductivity in sr _2 ruo _4. *arXiv preprint arXiv:1912.09525*, 2019.

[37] Guoren Zhang, Evgeny Gorelov, Esmaeel Sarvestani, and Eva Pavarini. Fermi surface of sr 2 ruo 4: spin-orbit and anisotropic coulomb interaction effects. *Physical review letters*, 116(10): 106402, 2016.

[38] A. Tamai, M. Zingl, E. Rozbicki, E. Cappelli, S. Riccò, A. de la Torre, S. McKeown Walker, F. Y. Bruno, P. D. C. King, W. Meevasana, M. Shi, M. Radović, N. C. Plumb, A. S. Gibbs, A. P. Mackenzie, C. Berthod, H. U. R. Strand, M. Kim, A. Georges, and F. Baumberger. High-resolution photoemission on sr_2ruo_4 reveals correlation-enhanced effective spin-orbit coupling and dominantly local self-energies. *Phys. Rev. X*, 9:021048, Jun 2019. doi:10.1103/PhysRevX.9.021048. URL `https://link.aps.org/doi/10.1103/PhysRevX.9.021048`.

[39] S. A. Kivelson, Andrew C. Yuan, B. J. Ramshaw, and Ronny Thomale. A proposal for reconciling diverse experiments on the superconducting state in sr _2 ruo _4. 2020.

[40] S. Raghu, E. Berg, A. V. Chubukov, and S. A. Kivelson. Effects of longer-range interactions on unconventional superconductivity. *Phys. Rev. B*, 85:024516, Jan 2012. doi: 10.1103/PhysRevB.85.024516. URL `https://link.aps.org/doi/10.1103/PhysRevB.85.024516`.

[41] Jake S. Bobowski, Naoki Kikugawa, Takuto Miyoshi, Haruki Suwa, Han-shu Xu, Shingo Yonezawa, Dmitry A. Sokolov, Andrew P. Mackenzie, and Yoshiteru Maeno. Improved single-crystal growth of sr2ruo4. *Condensed Matter*, 4(1), 2019. ISSN 2410-3896. doi: 10.3390/condmat4010006. URL `https://www.mdpi.com/2410-3896/4/1/6`.

[42] A. P. Mackenzie, R. K. W. Haselwimmer, A. W. Tyler, G. G. Lonzarich, Y. Mori, S. Nishizaki, and Y. Maeno. Extremely strong dependence of superconductivity on disorder in sr_2ruo_4. *Phys. Rev. Lett.*, 80:161–164, Jan 1998. doi:10.1103/PhysRevLett.80.161. URL `https://link.aps.org/doi/10.1103/PhysRevLett.80.161`.

[43] Arkady Shekhter, B. J. Ramshaw, Ruixing Liang, W. N. Hardy, D. A. Bonn, Fedor F. Balakirev, Ross D. McDonald, Jon B. Betts, Scott C. Riggs, and Albert Migliori. Bounding the pseudogap with a line of phase transitions in $YBa_2Cu_3O_{6+\delta}$. *Nature*, 498:75 EP –, Jun 2013. URL `https://doi.org/10.1038/nature12165`.

[44] D. Forsythe, S. R. Julian, C. Bergemann, E. Pugh, M. J. Steiner, P. L. Alireza, G. J. McMullan, F. Nakamura, R. K. W. Haselwimmer, I. R. Walker, S. S. Saxena, G. G. Lonzarich, A. P. Mackenzie, Z. Q. Mao, and Y. Maeno. Evolution of fermi-liquid interactions in sr_2ruo_4 under pressure. *Phys. Rev. Lett.*, 89:166402, Sep 2002. doi:10.1103/PhysRevLett.89.166402. URL `https://link.aps.org/doi/10.1103/PhysRevLett.89.166402`.

[45] K. Fossheim and B. Berre. Ultrasonic propagation, stress effects, and interaction parameters at the displacive transition in $srtio_3$. *Phys. Rev. B*, 5:3292–3308, Apr 1972. doi: 10.1103/PhysRevB.5.3292. URL `https://link.aps.org/doi/10.1103/PhysRevB.5.3292`.

[46] Clifford W. Hicks, Daniel O. Brodsky, Edward A. Yelland, Alexandra S. Gibbs, Jan A. N. Bruin, Mark E. Barber, Stephen D. Edkins, Keigo Nishimura, Shingo Yonezawa, Yoshiteru Maeno, and Andrew P. Mackenzie. Strong increase of tc of sr2ruo4 under both tensile and compressive strain. *Science*, 344(6181):283–285, 2014. ISSN 0036-8075. doi: 10.1126/science.1248292. URL `https://science.sciencemag.org/content/344/6181/283`.

[47] Y. S. Li, N. Kikugawa, D. A. Sokolov, F. Jerzembeck, A. S. Gibbs, Y. Maeno, C. W. Hicks, M. Nicklas, and A. P. Mackenzie. High precision heat capacity measurements on Sr2RuO4 under uniaxial pressure. *arXiv e-prints*, art. arXiv:1906.07597, Jun 2019.

SUPPLEMENTARY INFORMATION

Materials and Methods

High-quality single crystalline Sr_2RuO_4 samples were grown by floating-zone method, details of which can be found in [41]. A single crystal was oriented along [110], [1$\bar{1}$0] and [001] directions, and polished to dimensions 1.50mm $\times$ 1.60mm $\times$ 1.44mm, with 1.44mm along the tetragonal c-axis. The [110] orientation of the crystal was accounted for when solving for the elastic moduli.

Sample Characterization

The quality of the Sr_2RuO_4 rod, from which the sample was cut, was characterized by heat capacity and AC susceptibility measurements, shown in Figure 4. Heat capacity measurements of a large piece of Sr_2RuO_4 exhibit a T_c around 1.45 K, which is close to the optimal T_c [42]. Additional to a large T_c, a low concentration of ruthenium inclusions was an important criterion for the selection of a sample. Ruthenium inclusions locally strain the crystal lattice and thereby can enhance T_c up to 3 K. In order to check for ruthenium inclusions, we measured AC susceptibility by a mutual inductance method, which found a sharp onset-Tc of 1.43 K, indicating a very low concentration of ruthenium inclusions. These variations in T_c arise since the samples for specific heat and AC susceptibility were taken from different parts of the same Sr_2RuO_4 rod. The Sr_2RuO_4 sample for the RUS experiments was also taken from the same rod, and superconductivity is seen to onset at 1.42 K, which is in good agreement with the above-mentioned probes of T_c.

Low-temperature RUS

The relatively low T_c of Sr_2RuO_4 poses several challenges to perform RUS experiments through the superconducting transition. Since RUS samples are typically large ($\sim$ 1 mm^3) and not glued to the transducers (to ensure free boundary conditions), there is weak thermal contact between the sample and its surroundings. Hence, when cooled through T_c, the entire sample may not become superconducting at once, leading to broad superconducting transitions rather than sharp jumps at T_c. To cool below 4.2 K, one could introduce liquid

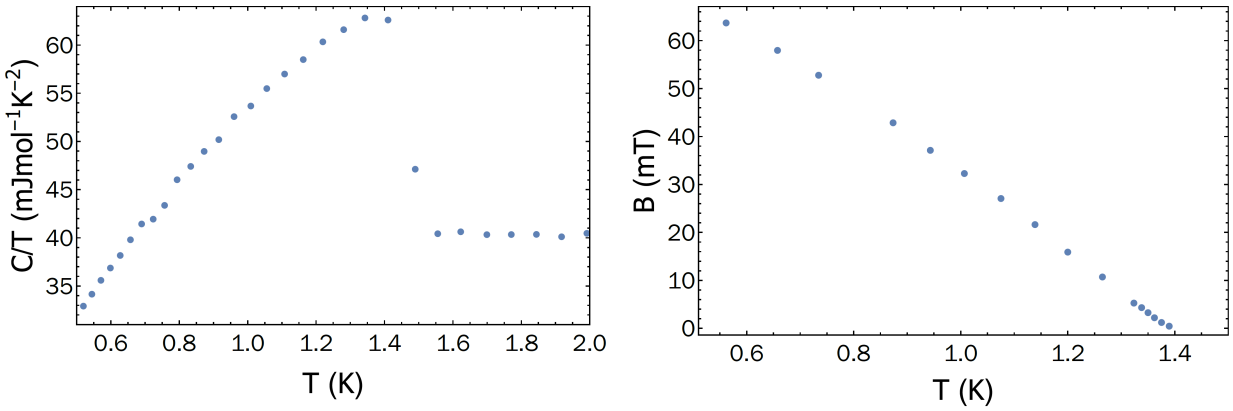

FIG. 4. T_c **variation within Sr_2RuO_4 rod.** (a) Specific heat and (b) critical field measured on different parts of the same rod from which the sample for RUS experiment was obtained. T_c is seen to vary by about 100 mK between different parts of the rod.

helium into the sample space and pump directly on this space. As RUS is extremely sensitive to vibration, however, this introduces artifacts into the data, and does not provide a particularly homogeneous thermal environment.

To solve these problems the RUS probe was sealed inside a copper can with a small amount of exchange gas, providing good thermal equilibration between the sample, thermometer, and the rest of the apparatus. This inner copper can is separated by a weak thermal link (thin-wall stainless) from an outer brass vacuum can, which provided isolation between the walls of the sample can and the bath. The temperature was regulated by pumping on the external helium bath, and the vacuum isolation of the sample chamber from the bath allows the sample space to then cool very slowly once the bath is pumped to base temperature.

The lowest temperature reached was approximately 1.25 K, as read by a CX-1030 thermometer affixed to the RUS probe. The transition temperature and transition width observed by RUS agree extremely well with those determined from independent susceptibility measurements, suggesting that the Sr_2RuO_4 sample was uniformly thermalized during the experiment.

Strain-Order Parameter Coupling

In this section, we calculate expressions for the elastic moduli discontinuities and attenuation, starting from a Ginzburg-Landau theory. Similar expressions for the chiral state have

been calculated by Sigrist [21] and for nematic superconducting states by Huang et al. [22]. Our expressions match those of Sigrist for the chiral state, and we correct the expressions derived by Huang et al. by including all possible order parameter fluctuations. In particular, we find that both in-plane shear moduli ($(c_{11} - c_{12})/2$ and c_{66}) should show a discontinuity for the nematic states, contrary to what was concluded in [22]. We also show that the three A_{1g} jumps always follow a consistency relation, similar to what was concluded for non-superconducting order parameters in URu_2Si_2[17], which is also a tetragonal material with point group D_{4h}.

For a two-component superconducting order parameter $\boldsymbol{\eta} = (\eta_x, \eta_y)$, the Landau free energy expansion reads

$$\mathcal{F}_{op}(\boldsymbol{\eta}) = a|\boldsymbol{\eta}|^2 + b_1|\boldsymbol{\eta}|^4 + \frac{b_2}{2}\Big((\eta_x^*\eta_y)^2 + (\eta_x\eta_y^*)^2\Big) + b_3|\eta_x|^2|\eta_y|^2 + ... \tag{3}$$

where $a = a_0(T - T_c)$, with $a_0 > 0$, and b_i are phenomenological constants. In a tetragonal crystal, the elastic free energy density is given by

$$\begin{aligned}\mathcal{F}_{el} &= \frac{1}{2}\Big(c_{11}(\epsilon_{xx}^2 + \epsilon_{yy}^2) + 2c_{12}\epsilon_{xx}\epsilon_{yy} + c_{33}\epsilon_{zz}^2 + 2c_{13}(\epsilon_{xx} + \epsilon_{yy})\epsilon_{zz} + 4c_{44}(\epsilon_{xz}^2 + \epsilon_{yz}^2) + 4c_{66}\epsilon_{xy}^2\Big) \\ &= \frac{1}{2}\Big(\frac{c_{11} + c_{12}}{2}(\epsilon_{xx} + \epsilon_{yy})^2 + c_{33}\epsilon_{zz}^2 + 2c_{13}(\epsilon_{xx} + \epsilon_{yy})\epsilon_{zz} + \frac{c_{11} - c_{12}}{2}(\epsilon_{xx} - \epsilon_{yy})^2 + \\ &\quad 4c_{44}(\epsilon_{xz}^2 + \epsilon_{yz}^2) + 4c_{66}\epsilon_{xy}^2\Big) \\ &= \frac{1}{2}\Big(c_{A_{1g},1}\epsilon_{A_{1g},1}^2 + c_{A_{1g},2}\epsilon_{A_{1g},2}^2 + 2c_{A_{1g},3}\epsilon_{A_{1g},1}\epsilon_{A_{1g},2} + c_{B_{1g}}\epsilon_{B_{1g}}^2 + c_{E_g}|\epsilon_{E_g}|^2 + c_{B_{2g}}\epsilon_{B_{2g}}^2\Big)\end{aligned} \tag{4}$$

where the strains are written as the irreducible representations of D_{4h}, $(\epsilon_{xx} + \epsilon_{yy}) \to \epsilon_{A_{1g},1}$, $\epsilon_{zz} \to \epsilon_{A_{1g},2}$, $(\epsilon_{xx} - \epsilon_{yy}) \to \epsilon_{B_{1g}}$, $2\epsilon_{xy} \to \epsilon_{B_{2g}}$ and $(2\epsilon_{xz}, 2\epsilon_{yz}) \to \epsilon_{E_g}$.

The lowest order terms that couple strain to the superconducting order parameter must be quadratic in order parameter to preserve gauge symmetry. This coupling gives rise to additional contributions to the free energy

$$\mathcal{F}_c = (g_1\epsilon_{A_{1g},1} + g_2\epsilon_{A_{1g},2})|\boldsymbol{\eta}|^2 + g_4\epsilon_{B_{1g}}(|\eta_x|^2 - |\eta_y|^2) + g_5\epsilon_{B_{2g}}(\eta_x^*\eta_y + \eta_x\eta_y^*), \tag{5}$$

where g_i are coupling constants. Coupling between OP and B_{1g}, B_{2g} strains are only allowed for two-component OPs; one-component OPs can only couple to compressive strains (shown for example gap structures in Figure 5). These linear-in-strain, quadratic-in-order-parameter coupling lead to elastic moduli jumps at T_c. Hence jumps in shear moduli can only occur

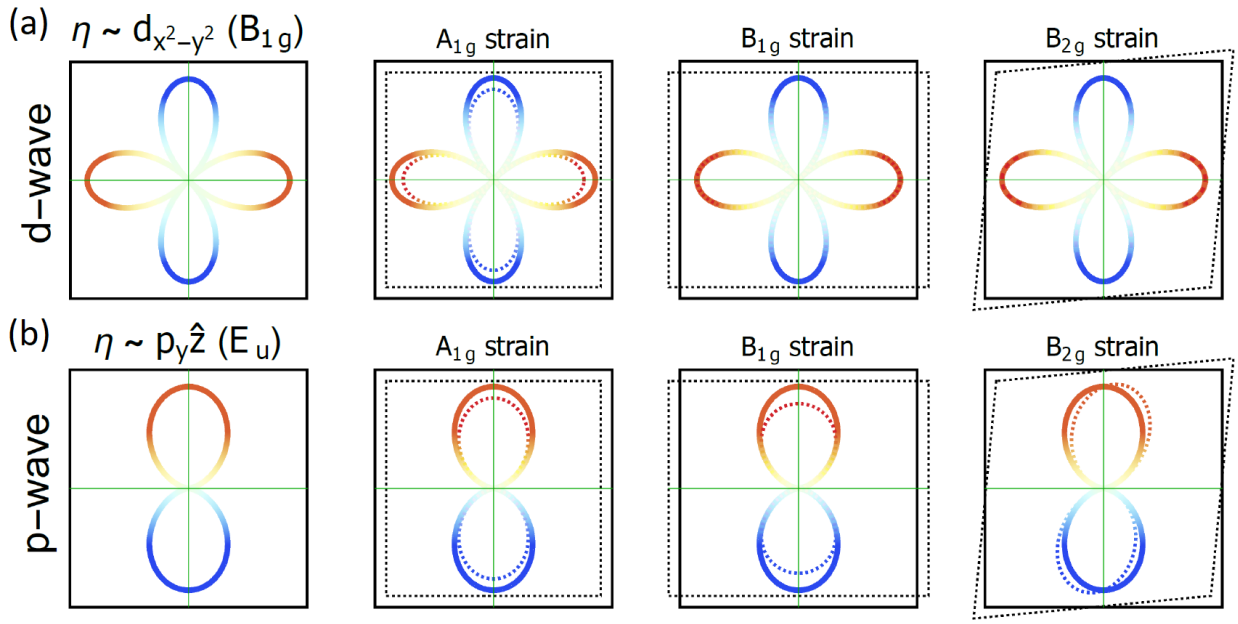

FIG. 5. **Coupling between strain and one/two component order parameters.** (a) Structure of $d_{x^2-y^2}$ gap and (b) $p_y\hat{\boldsymbol{z}}$ gap in k-space, and their couplings to strain. $\hat{\boldsymbol{z}}$ represents the pair wavefunction in spin space. Allowed couplings modify the gap structure in k-space. Only A_{1g} strain couples to one-component order parameters, while A_{1g}, B_{1g} and B_{2g} strain all couple to two-component order parameters.

if the OP is two-component. Since no OP can couple to E_g strain, c_{44} should not show a jump at T_c for any superconducting order parameter.

Following Sigrist[21], we use the parameterization $\boldsymbol{\eta} = (\eta_x, \eta_y) = \eta(\cos\theta, e^{i\gamma}\sin\theta)$. Depending on the relative magnitudes of b_1, b_2, b_3, the system can have different equilibrium OPs[22], characterized by different equilibrium values of $(\theta, \gamma) = (\theta_0, \gamma_0)$: $(\pi/4, \pm\pi/2)$ for the chiral state, $(\pi/4, 0)$ for the diagonal nematic state and $(0, 0)$ for the horizontal nematic state. These states also have different equilibrium values of $\eta = \eta_0$, which can be calculated from $\partial\mathcal{F}_{op}/\partial\eta|_{(\theta,\gamma)\to(\theta_0,\gamma_0)} = 0$. Fluctuations of the order parameter amplitude η, orientation θ or relative phase γ can couple to different strains, leading to the jump in corresponding moduli.

To explicitly calculate the moduli discontinuities, we adapt the approach described in [43] to a multi-component OP. For one-component OPs, the discontinuity is

$$c^{<}_{mn} = c^{>}_{mn} - \frac{Z_m Z_n}{Y} \implies \Delta c_{mn} = c^{>}_{mn} - c^{<}_{mn} = \frac{Z_m Z_n}{Y} \tag{6}$$

where $c^{<}_{mn}(c^{>}_{mn})$ is the elastic modulus below(above) T_c. The thermodynamic coefficients Z_i, Y are defined as $Z_i = \partial^2\mathcal{F}_c/\partial\eta\partial\epsilon_i$ and $Y = \partial^2\mathcal{F}_{op}/\partial\eta^2$. For a multi-component OP $\boldsymbol{\eta}$, Equation 6 gets modified to

$$\Delta c_{mn} = \boldsymbol{Z_m^T Y^{-1} Z_n} \tag{7}$$

where $\boldsymbol{Z_i} = \partial^2\mathcal{F}_c/\partial\boldsymbol{\eta}\partial\epsilon_i$ and $\boldsymbol{Y} = \partial^2\mathcal{F}_{op}/\partial\boldsymbol{\eta}^2$ are now matrices. Within this formalism, one can find which OP fluctuation mode couples to a particular strain by looking at the Z_i for that strain. For example, for the chiral state,

$$Z_{A_{1g},1(2)} = \begin{pmatrix} g_{1(2)}\sqrt{\frac{-8a}{4b_1-b_2+b_3}} \\ 0 \\ 0 \end{pmatrix}; Z_{B_{1g}} = \begin{pmatrix} 0 \\ g_4\frac{4a}{4b_1-b_2+b_3} \\ 0 \end{pmatrix}; Z_{B_{2g}} = \begin{pmatrix} 0 \\ 0 \\ g_5\frac{2a}{4b_1-b_2+b_3} \end{pmatrix} \tag{8}$$

This shows that η fluctuations couple to the A_{1g} strains, θ fluctuations couple to B_{1g} strain and γ fluctuations couple to B_{2g} strain, consistent with the conclusions of Sigrist [21].

The elastic moduli discontinuities for the various OPs is summarized in Table II. In all cases, the three A_{1g} jumps are found to satisfy the relation

$$\Delta c_{A_{1g},1} \times \Delta c_{A_{1g},2} = (\Delta c_{A_{1g},3})^2 \tag{9}$$

Using the measured jumps in $(c_{11}+c_{12})/2$, c_{33}, and c_{13} (see Figure 3 and Equation 4), we obtain $(\Delta\frac{c_{11}+c_{12}}{2}) \times (\Delta c_{33}) = (8\pm1)\times10^{-5}$ GPa^2, which is in agreement with $(\Delta c_{13})^2 = (7\pm1)\times10^{-5}$ GPa^2.

We now turn to order parameter dynamics near the phase transition, which can cause smearing of the frequency jumps. We start with the idea outlined in [43], and adapt it to a multi-component OP. Below T_c, the order parameter relaxation can be modeled as

$$\frac{\partial\tilde{\boldsymbol{\eta}}}{\partial t} = -\boldsymbol{\xi}\frac{\partial\mathcal{F}}{\partial\tilde{\boldsymbol{\eta}}} = -\boldsymbol{\xi}\Big(\frac{\partial^2\mathcal{F}}{\partial\boldsymbol{\eta}^2}\tilde{\boldsymbol{\eta}} + \sum_m \frac{\partial^2\mathcal{F}}{\partial\boldsymbol{\eta}\partial\epsilon_m}\epsilon_m\Big) = -\boldsymbol{\xi}\Big(\boldsymbol{Y}\tilde{\boldsymbol{\eta}} + \sum_m \boldsymbol{Z_m}\epsilon_m\Big) \tag{10}$$

where $\tilde{\boldsymbol{\eta}}$ are the fluctuations of OP components about equilibrium, and $-\boldsymbol{\xi}\frac{\partial\mathcal{F}}{\partial\tilde{\boldsymbol{\eta}}}$ provides the restoring force towards equilibrium. Assuming linear response of OP fluctuations to strain, when strain is modulated at frequency ω, as in a RUS experiment, Equation 10 becomes

$$-i\omega\tilde{\boldsymbol{\eta}}(\omega) = -\boldsymbol{\tau}^{-1}\tilde{\boldsymbol{\eta}}(\omega) - \boldsymbol{\xi}\sum_m \boldsymbol{Z_m}\epsilon_m \implies \tilde{\boldsymbol{\eta}}(\omega) = (i\omega\boldsymbol{\tau} - \mathbb{1})^{-1}\boldsymbol{Y}^{-1}\sum_m \boldsymbol{Z_m}\epsilon_m \tag{11}$$

OP	Chiral	Diagonal Nematic	Horizontal Nematic
(θ_0, γ_0)	$(\pi/4, \pm\pi/2)$	$(\pi/4, 0)$	$(0, 0)$
η_0	$\sqrt{\frac{-2a}{4b_1-b_2+b_3}}$	$\sqrt{\frac{-2a}{4b_1+b_2+b_3}}$	$\sqrt{\frac{-a}{2b_1}}$
$\Delta c_{A_{1g},1}$	$\frac{2g_1^2}{4b_1-b_2+b_3}$ (η)	$\frac{2g_1^2}{4b_1+b_2+b_3}$ (η)	$\frac{g_1^2}{2b_1}$ (η)
$\Delta c_{A_{1g},2}$	$\frac{2g_2^2}{4b_1-b_2+b_3}$ (η)	$\frac{2g_2^2}{4b_1+b_2+b_3}$ (η)	$\frac{g_2^2}{2b_1}$ (η)
$\Delta c_{A_{1g},3}$	$\frac{2g_1g_2}{4b_1-b_2+b_3}$ (η)	$\frac{2g_1g_2}{4b_1+b_2+b_3}$ (η)	$\frac{g_1g_2}{2b_1}$ (η)
$\Delta c_{B_{1g}}$	$\frac{2g_4^2}{b_2-b_3}$ (θ)	$\frac{-2g_4^2}{b_2+b_3}$ (θ)	$\frac{g_4^2}{2b_1}$ (η)
$\Delta c_{B_{2g}}$	$\frac{g_5^2}{b_2}$ (γ)	$\frac{2g_5^2}{4b_1+b_2+b_3}$ (η)	$\frac{2g_5^2}{b_2+b_3}$ (θ)

TABLE II. Different equilibrium order parameters and the discontinuities they produce in various elastic moduli. In parentheses, we note fluctuation of which OP mode couples to ultrasound. Jump in compressional (A_{1g}) moduli is always caused by amplitude (η) fluctuations of the OP, whereas for shear modes, jumps can arise from coupling to amplitude (η), orientation (θ) or relative phase (γ) fluctuations.

where we have defined $\boldsymbol{\tau}^{-1} = \boldsymbol{\xi}\boldsymbol{Y}$ is the matrix of relaxation times for independent OP modes. For the parameterization $\boldsymbol{\eta} = \eta(\cos\theta, e^{i\gamma}\sin\theta)$,

$$\boldsymbol{\tau} = \begin{pmatrix} \tau_\eta & 0 & 0 \\ 0 & \tau_\theta & 0 \\ 0 & 0 & \tau_\gamma \end{pmatrix} \implies (i\omega\boldsymbol{\tau} - \mathbb{1})^{-1} = \begin{pmatrix} (i\omega\tau_\eta - 1)^{-1} & 0 & 0 \\ 0 & (i\omega\tau_\theta - 1)^{-1} & 0 \\ 0 & 0 & (i\omega\tau_\gamma - 1)^{-1} \end{pmatrix} \tag{12}$$

Using Equation 11, we calculate the dynamic elastic constant as,

$$c_{mn}(\omega) = c^{>}_{mn} + \frac{\partial^2\mathcal{F}}{\partial\boldsymbol{\eta}\partial\epsilon_m}\frac{\partial\tilde{\boldsymbol{\eta}}}{\partial\epsilon_n} \implies c^{<}_{mn}(\omega) = c^{>}_{mn} + \boldsymbol{Z}^T_{\boldsymbol{m}}(i\omega\boldsymbol{\tau} - \mathbb{1})^{-1}\boldsymbol{Y}^{-1}\boldsymbol{Z}_{\boldsymbol{n}} \tag{13}$$

Elastic moduli jumps come from the real part of Equation 13. Depending on which OP mode a particular elastic moduli couples to, the modulus dispersion $c_{mn}(\omega)$ picks up a contribution from the corresponding relaxation time. For example, for the chiral OP,

$$\Delta c_{A_{1g},1(2)} = \frac{2g^2_{1(2)}}{4b_1 - b_2 + b_3}\frac{1}{1+\omega^2\tau_\eta^2}; \Delta c_{B_{1g}} = \frac{2g_4^2}{b_2 - b_3}\frac{1}{1+\omega^2\tau_\theta^2}; \Delta c_{B_{2g}} = \frac{g_5^2}{b_2}\frac{1}{1+\omega^2\tau_\gamma^2}$$

Thus OP relaxation effects can broaden out the elastic moduli jumps, if particular relaxation times are long compared to the experimental frequencies. Since we measure non-zero discontinuities in all the A_{1g} moduli, and the B_{2g} modulus, but no jump in B_{1g} modulus,

it is plausible that the B_{1g} jump gets strongly smeared due to this effect. Specifically, for the diagonal nematic state, only the B_{1g} jump is affected by τ_θ, while the other 4 jumps are related to τ_η. Hence if τ_θ is much larger than τ_η for this state, it provides an explanation for the lack fo B_{1g} jump. We also note that for this state, close to T_c $(1 - T/T_c \ll 1)$, $\tau_\eta^{-1} \propto |a| \propto \eta_0^2 \propto (T_c - T)$ and $\tau_\theta^{-1} \propto \eta_0^4 \propto (T_c - T)^2$. This would indeed make τ_θ much longer than τ_η just below T_c. We also note that large ultrasonic attenuation is observed experimentally in the B_{1g} channel [19], which perhaps motivates the presence of such a long relaxation time.

Ehrenfest Relations for Compressional Strains

At the superconducting transition, a jump discontinuity is also measured in the specific heat. Within our formalism, the specific heat jump at T_c, $\Delta C/T$, is calculated as

$$\frac{\Delta C}{T} = \boldsymbol{W}^T \boldsymbol{Y}^{-1} \boldsymbol{W} \tag{14}$$

where $\boldsymbol{W} = \partial^2 \mathcal{F}_{op}/\partial \boldsymbol{\eta} \partial T$ and $\boldsymbol{Y} = \partial^2 \mathcal{F}_{op}/\partial \boldsymbol{\eta}^2$. For all three superconducting states discussed above, the A_{1g} moduli jumps can be related to the specific heat jump through

$$\Delta c_{A_{1g},1(2)} = -\frac{\Delta C}{T}\left(\frac{dT_c}{d\epsilon_{A_{1g},1(2)}}\right)^2; \Delta c_{A_{1g},3} = -\frac{\Delta C}{T}\left|\frac{dT_c}{d\epsilon_{A_{1g},1}}\right|\left|\frac{dT_c}{d\epsilon_{A_{1g},2}}\right| \tag{15}$$

It is important to note that such relations for the shear strains are more complicated, and we derive them in the next section. For a tetragonal material, the bulk modulus B is related to the three A_{1g} moduli as

$$B = \frac{\left(\frac{c_{11}+c_{12}}{2}\right)c_{33} - c_{13}^2}{\left(\frac{c_{11}+c_{12}}{2}\right) + c_{33} - 2c_{13}} \tag{16}$$

From Equation 15,the discontinuity in the bulk modulus $\Delta B/B$ at T_c can be related to $\Delta C/T$ through the Ehrenfest relation

$$\frac{\Delta B}{B^2} = -\frac{\Delta C}{T}\left(\frac{dT_c}{dP_{hyd}}\right)^2 \tag{17}$$

where dT_c/dP_{hyd} is the hydrostatic pressure dependence of T_c. Our measurements give $\Delta B/B \sim 5.9 \times 10^{-5}$, about 8.4 times larger than estimated from specific heat jump and dT_c/dP_{hyd} [44] or, alternatively, the measured jump in the bulk modulus predicts dT_c/dP_{hyd} to be a factor of 2.9 higher than the measured value. This discrepancy can arise due to

the formation of order parameter domains [45], which lead to an additional slowing down of ultrasound and therefore a larger drop in the elastic moduli through T_c. Since these domains would be related to each other by time-reversal in a superconductor, however, it is unclear whether such a mechanism would couple strongly to ultrasound. Another possible cause could be the value of dT_c/dP_{hyd} estimated from the data in [44]. Since the T_c of Sr_2RuO_4 shows a strong increase with B_{1g} strain[46], the measured decrease in T_c under P_{hyd} will be less if the pressure applying medium is not completely hydrostatic. This is particularly relevant because the B_{1g} modulus is almost 4 times smaller than $(c_{11} + c_{12})/2$, which makes it easy to induce B_{1g} strain if the pressure medium is not hydrostatic. Finally, with the possible discovery of two transitions occurring either simultaneously or near-simultaneously at T_c, it will be necessary to map out T_{TRSB} with pressure to correctly calculate the Ehrenfest relations, which are modified under the presence of two accidentally degenerate order parameters [39].

Ehrenfest Relations for Shear Strains

Unlike A_{1g} strains, shear strains (B_{1g} and B_{2g}) are expected to split the superconducting transition if the OP is a symmetry-protected multi-component order parameter [46]. This happens because shear strains break the tetragonal symmetry of the lattice, and hence the degenerate OP components of the unstrained crystal now have different condensation energies (and temperatures). Within weak coupling, a crystal under shear strain should therefore show two specific heat jumps[47], and, for a chiral OP, time-reversal symmetry breaking (TRSB) should set in at a different temperature than Meissner effect. Recent μSR experiments[27] have indeed reported the latter effect. We show that the shear modulus jump can be related to $\Delta C/T$ (at zero strain) through the strain derivatives of these two transition temperatures, T_c and T_{TRSB},

$$\Delta c_s = -\frac{\Delta C}{T}\left|\frac{dT_1}{d\epsilon_s}\right|\left|\frac{dT_2}{d\epsilon_s}\right|, \tag{18}$$

where s is either B_{1g} or B_{2g}, $T_1 = T_c$, and $T_2 = T_{TRSB}$.

We start from the free energy expressions $\mathcal{F}_{op}$ and $\mathcal{F}_c$, and consider the case $b_2 > 0, b_3 < b_2$, which leads to a chiral OP. Further, we keep only the coupling to $\epsilon_{B_{1g}}$ to simplify the

subsequent algebra. Then, with the phase between η_x and η_y set to $\pi/2$, $\mathcal{F}_{op}$ and $\mathcal{F}_c$ are

$$\begin{aligned}\mathcal{F}_{op} &= a_0(T - T_{c,0})(\eta_x^2 + \eta_y^2) + b_1(\eta_x^2 + \eta_y^2)^2 + (b_3 - b_2)\eta_x^2\eta_y^2 \\ \mathcal{F}_c &= g_4\epsilon_{B_{1g}}(\eta_x^2 - \eta_y^2),\end{aligned} \tag{19}$$

where $T_{c,0}$ is the unstrained T_c. Clearly, $\epsilon_{B_{1g}}$ breaks the $\eta_x \leftrightarrow \eta_y$ symmetry of the quadratic terms in free energy, thereby making the two components condense at different temperatures.

We assume $g_4\epsilon_{B_{1g}} > 0$, which favors η_y condensing before η_x. The higher transition temperature $T_1 = T_\mathrm{c}$ is determined by when the coefficient of η_y^2 goes to zero (with $\eta_x = 0$), that is, $a_0(T_1 - T_{c,0}) - g_4\epsilon_{B_{1g}} = 0$. This gives

$$T_1 = T_{c,0} + \frac{g_4}{a_0}\epsilon_{B_{1g}}. \tag{20}$$

Then, the η_y that minimizes $(\mathcal{F}_{op} + \mathcal{F}_c)$ is

$$\eta_y^2 = \frac{a_0(T_{c,0} - T) + g_4\epsilon_{B_{1g}}}{2b_1} = \frac{a_0(T_1 - T)}{2b_1}. \tag{21}$$

Further, the specific heat jump at this transition, calculated by using the above η_y^2, is

$$\left(\frac{\Delta C}{T}\right)_1 = \frac{a_0^2}{2b_1}. \tag{22}$$

Below T_1, the system undergoes TRSB transition when η_x condenses. Naively, one might expect this to occur at $T_{c,0} - g_4\epsilon_{B_{1g}}/a_0$, found by setting the quadratic coefficient of η_x to zero. The condensation of η_y prevents this, however, through the $\eta_x^2\eta_y^2$ terms in $\mathcal{F}_{op}$. If the coefficient of this term is zero ($2b_1 + b_3 - b_2 = 0$), then there is no competition between η_x and η_y, in which case the second transition does occur at $T_{TRSB} = T_{c,0} - g_4\epsilon_{B_{1g}}/a_0$.

For the more general case, when $2b_1 + b_3 - b_2 \neq 0$, $T_2 = T_{TRSB}$ is calculated by setting the coefficient of η_x^2 to zero in the total free energy, with η_y given by Equation 21. This gives

$$\begin{aligned}a_0(T_2 - T_{c,0}) + (2b_1 + b_3 - b_2)\eta_y^2 + g_4\epsilon_{B_{1g}} &= 0 \\ \implies T_2 = T_{c,0} - \frac{g_4}{a_0}\left(\frac{4b_1 - b_2 + b_3}{b_2 - b_3}\right)\epsilon_{B_{1g}}\end{aligned} \tag{23}$$

The specific heat jump at this transition can be calculated by subtracting the jump in first transition $(\Delta C/T)_1$ from the total jump $\Delta C/T$ in the unstrained case.

$$\left(\frac{\Delta C}{T}\right)_2 = \frac{2a_0^2}{4b_1 - b_2 + b_3} - \frac{a_0^2}{2b_1} = \frac{a_0^2}{2b_1}\frac{b_2 - b_3}{4b_1 - b_2 + b_3} \tag{24}$$

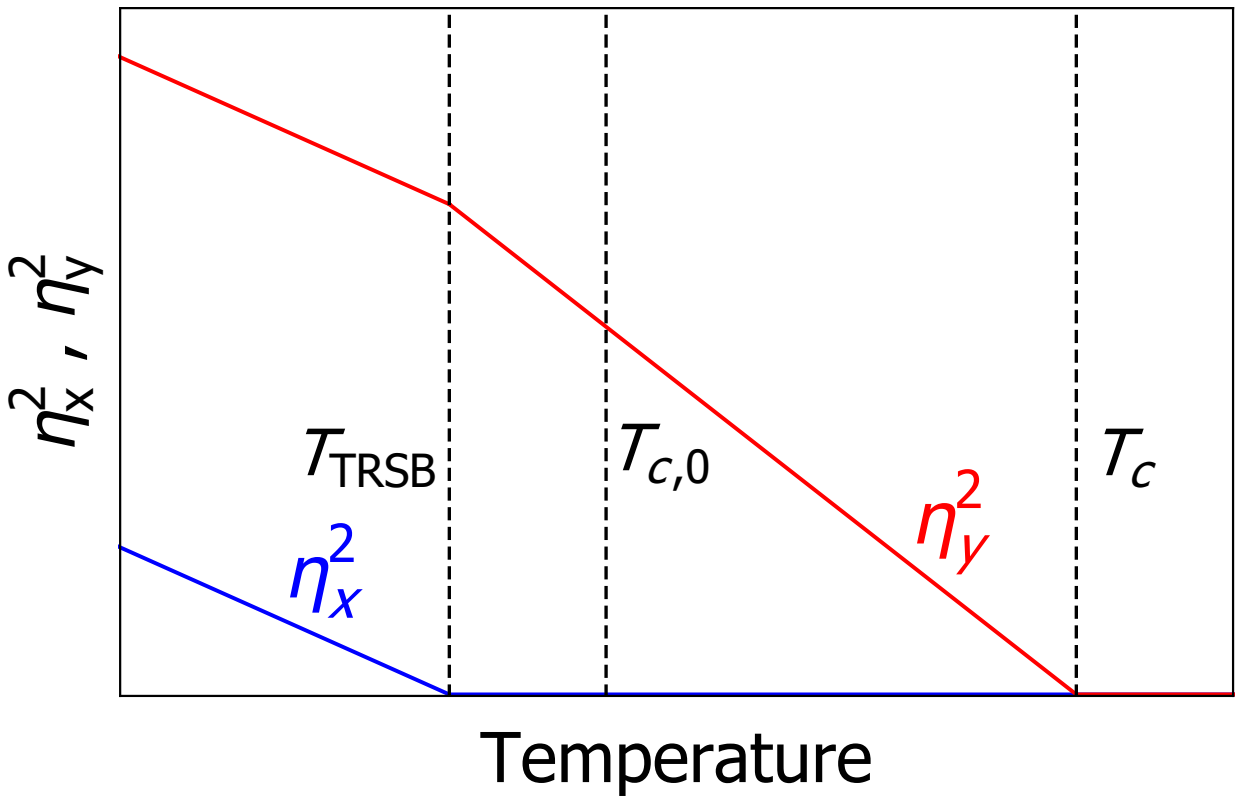

FIG. 6. **Strain-induced splitting of the transition temperature $T_{c,0}$.** Under B_{1g} shear strain, the two components η_y and η_x condense at different temperatures, T_c and T_{TRSB}, respectively. Above T_c, both the components are zero, and the sample is not superconducting. At T_c, the Meissner effect sets in, and finally, below T_{TRSB}, the system becomes a chiral superconductor. Note that the condensation of η_x decreases the rate at which η_y was growing below T_c. Qualitatively similar behavior is expected for B_{2g} shear strain, see text for details.

The ratio of the two specific heat jumps can then be related by

$$\left(\frac{\Delta C}{T}\right)_1 \Big/ \left(\frac{\Delta C}{T}\right)_2 = \frac{4b_1 - b_2 + b_3}{b_2 - b_3} = \left|\frac{dT_2}{d\epsilon_{B_{1g}}}\right| \Big/ \left|\frac{dT_1}{d\epsilon_{B_{1g}}}\right| \tag{25}$$

Below T_2, the order parameter (η_x, η_y) can be calculated by minimizing $(\mathcal{F}_{op} + \mathcal{F}_c)$ with respect to both η_x and η_y. This gives

$$\begin{aligned} \eta_x^2 &= \frac{a_0(T_2 - T)}{4b_1 - b_2 + b_3} \\ \eta_y^2 &= \frac{a_0}{2b_1}\left((T_1 - T) - \frac{2b_1 - b_2 + b_3}{4b_1 - b_2 + b_3}(T_2 - T)\right) \end{aligned} \tag{26}$$

It is interesting to note that the condensation of η_x at T_2 decreases the rate at which η_y was growing below T_1, demonstrating the competition between the two components.

The jump in the B_{1g} shear modulus for chiral OP can now be expressed as,

$$\Delta c_{B_{1g}} = \frac{2g_4^2}{b_2 - b_3} = \frac{2a_0^2}{4b_1 - b_2 + b_3} \cdot \frac{g_4}{a_0} \cdot \frac{g_4}{a_0}\left(\frac{4b_1 - b_2 + b_3}{b_2 - b_3}\right) = -\frac{\Delta C}{T}\left|\frac{dT_1}{d\epsilon_{B_{1g}}}\right|\left|\frac{dT_2}{d\epsilon_{B_{1g}}}\right| \tag{27}$$

A similar derivation can be carried out for B_{2g} strain. This can be performed simply by re-defining the order parameter variables as $\tilde{\eta}_x = (\eta_x + \eta_y)/\sqrt{2}$ and $\tilde{\eta}_y = (\eta_x - \eta_y)/\sqrt{2}$ and carrying out the same calculation as the B_{1g} case.

Reconciling the c_{66} Discontinuity with Previous Experiments

It follows from our measurement of a non-zero discontinuity in c_{66} that two transitions should occur under $\epsilon_{B_{2g}} = \epsilon_{xy}$ strain, each showing a specific heat jump, and T_c must split linearly with ϵ_{xy} strain (see Equation 20). However, past experiments[46, 47] have not observed either of these effects, and we comment on that here.

Experimental resolution of specific heat measurements under strain [47], and a lack of an observed discontinuity at a lower transition ($T_\mathrm{TRSB} \equiv T_2$) gives a bound on the ratio of specific heat jumps at the purported transitions 1 and 2 as,

$$\left(\frac{\Delta C}{T}\right)_1 \Big/ \left(\frac{\Delta C}{T}\right)_2 = \left|\frac{dT_2}{d\epsilon_{B_{2g}}}\right| \Big/ \left|\frac{dT_1}{d\epsilon_{B_{2g}}}\right| \geq 20. \tag{28}$$

From the jumps in the B_{2g} modulus, $\Delta c_{66} \approx 10^6$ Pa, and in the specific heat, $\Delta C/T = 25$ mJ mol^{-1} K^{-2} ≈ 450 J m^3 K^{-2}, we get

$$\left|\frac{dT_1}{d\epsilon_{B_{2g}}}\right|\left|\frac{dT_2}{d\epsilon_{B_{2g}}}\right| \approx 2000 \text{ K}^2. \tag{29}$$

From these two equations, we can estimate the shifts in the transition temperatures with strain as

$$\begin{aligned} \left|\frac{dT_1}{d\epsilon_{B_{2g}}}\right| &\leq 10 \text{ K} = 0.1 \text{ K}/\%_\mathrm{strain} \\ \left|\frac{dT_2}{d\epsilon_{B_{2g}}}\right| &\geq 200 \text{ K} = 2 \text{ K}/\%_\mathrm{strain} \end{aligned} \tag{30}$$

We can now compare these estimates to what has been experimentally observed. T_c as a function of ϵ_{xy} was reported in Hicks et al. [46], and the resolution on a possible cusp was 0.1 K/%; therefore the data of Hicks et al. [46] do not rule out a cusp of the magnitude predicted here. Furthermore, in recent μSR experiments under applied B_{1g} strain[27], a modest suppression of T_{TRSB} is reported: ~ 0.2 K under a stress of -0.28 GPa, or a strain of $\sim -0.2\%$, for a slope of $\sim 1K/\%$. Although measurements under B_{2g} strain have not yet been reported, we note that this is comparable to the slope indicated above.